JVI Journals.ASM.org

Middle East Respiratory Syndrome Coronavirus Accessory Protein 4a Is a Type I Interferon Antagonist

Daniela Niemeyer,[a] Thomas Zillinger,[b] Doreen Muth,[a] Florian Zielecki,[c] Gabor Horvath,[d] Tasnim Suliman,[a] Winfried Barchet,[b] Friedemann Weber,[c] Christian Drosten,[a] Marcel A. Müller[a]

Institute of Virology, University of Bonn Medical Center, Bonn, Germany[a]; Institute of Clinical Chemistry and Clinical Pharmacology, University of Bonn Medical Center, Bonn, Germany[b]; Institute for Virology, Philipps University Marburg, Marburg, Germany[c]; Institute of Innate Immunity, University of Bonn Medical Center, Bonn, Germany[d]

Middle East respiratory syndrome coronavirus (MERS-CoV) causes severe acute respiratory infection with as yet unclear epidemiology. We previously showed that MERS-CoV counteracts parts of the innate immune response in human bronchiolar cells. Here we analyzed accessory proteins 3, 4a, 4b, and 5 for their abilities to inhibit the type I interferon response. Accessory protein 4a was found to block interferon induction at the level of melanoma differentiation-associated protein 5 (MDA5) activation presumably by direct interaction with double-stranded RNA.

The emerging Middle East respiratory syndrome coronavirus (MERS-CoV) (previously known as human coronavirus-Erasmus Medical Center HCoV-EMC/2012) and the related severe acute respiratory syndrome-associated CoV (SARS-CoV) are both linked to acute respiratory syndrome with severe outcomes, raising public health concerns (1–4). In contrast to other human-pathogenic CoV, MERS-CoV can replicate in cells from a broad range of mammalian species (5, 6). Its obvious zoonotic or even epidemic potential urges for the identification of MERS-CoV-specific virulence factors.

The capability of a virus to counteract the early innate immune response influences virus pathogenicity and clinical outcome in patients (7). The type I interferon (IFN) system plays a major role in antiviral innate immunity. It is commonly subdivided into the IFN induction pathway leading to IFN transcription and secretion, as opposed to the IFN signaling pathway resulting in the upregulation of antiviral proteins and the recruitment of immune cells following the secretion of cytokines (8, 9). Both SARS-CoV and MERS-CoV efficiently inhibit the activation of the type I IFN response (10, 11). Several IFN antagonistic proteins have been identified in SARS-CoV, including accessory proteins 3b and 6 (12–14). MERS-CoV has five putative accessory proteins (protein 3 [p3], p4a, p4b, p5, and p8b) with as yet unknown functions (15). In this study, we focused on p3, p4a, p4b, and p5 to investigate potential anti-IFN functions.

Promptly released genome sequence information (15) was used to predict putative protein localizations and motifs, including transmembrane domains using TMpred, glycosylation sites, and putative double-stranded RNA (dsRNA)-binding domains using DELTA-BLAST. Putative accessory proteins comprised 103 to 246 amino acids (aa) with expected molecular masses of 11 to 29 kDa (Table 1). The predicted topology of p3 and p4b revealed single transmembrane domains, whereas p5 had three putative transmembrane domains similar to the CoV structural membrane (M) protein (16). Interestingly, p4a had a predicted dsRNA-binding motif such as in IFN antagonists, including paramyxovirus V (17) and Ebola virus VP35 (18).

For heterologous expression and cellular protein localization studies, accessory open reading frames (ORFs) 3, 4a, and 4b were PCR amplified from MERS-CoV cDNA (primer sequences in Table S1 in the supplemental material), whereas ORF 5 was synthesized (Life Technologies). All ORFs were cloned into eukaryotic expression plasmid pCAGGS along with an N-terminal FLAG tag. For protein expression, human embryonic kidney HEK-293T cells were transfected with FuGENE HD (Promega). Expression of MERS-CoV accessory proteins was detected by immunofluorescence assay and Western blot analysis using an anti-FLAG immu-

Received 9 July 2013 **Accepted** 4 September 2013

Published ahead of print 11 September 2013

Address correspondence to Christian Drosten, drosten@virology-bonn.de, or Marcel A. Müller, muller@virology-bonn.de.

Supplemental material for this article may be found at http://dx.doi.org/10.1128/JVI.01845-13.

doi:10.1128/JVI.01845-13

TABLE 1 Features of MERS-CoV accessory proteins

Viral gene/protein	Genome positions (bp)	No. of amino acids	Predicted molecular mass (kDa)	Putative functional domain(s)[a]	Prediction of cellular localization/our observation[b]
ORF 3/p3	25,531–25,842	103	11	1 TMD, N-glycosylation site	Secretory pathway[c]/ERGIC and TGN
ORF 4a/p4a	25,851–26,180	109	12	dsRNA-binding domain	Signal peptide not found/cytoplasm and nucleus
ORF 4b/p4b	26,092–26,832	246	29	1 TMD	Nuclear localization signal[d]/cytoplasm and nucleus
ORF 5/p5	26,839–27,513	224	25	3 TMDs	Secretory pathway[c]/ERGIC

[a] Putative functional domain(s) were predicted by TMpred (40) and DELTA-BLAST (domain enhanced lookup time accelerated BLAST). TMD, transmembrane domain.
[b] ERGIC, endoplasmic reticulum-Golgi intermediate compartment; TGN, *trans*-Golgi network.
[c] Predicted by TargetP (41).
[d] Predicted by WoLF PSORT (42).

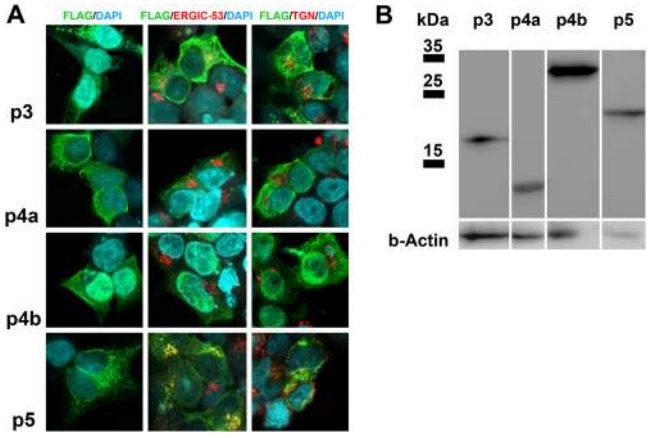

FIG 1 Expression and subcellular localization of MERS-CoV accessory proteins in HEK-293T cells. (A) The different accessory proteins 3, 4a, 4b, and 5 were expressed in HEK-293T cells, fixed after 24 h, and stained with a mouse anti-FLAG immunoglobulin G (IgG) for immunofluorescence assay analysis by confocal microscopy (Leica, SP5 SMD). A goat anti-mouse cyanine 2 (Cy2)-labeled IgG was used for secondary detection (shown in green). For colocalization studies, a rabbit anti-FLAG IgG followed by a goat anti-rabbit Cy2-conjugated IgG was used. As organelle marker antibodies, mouse anti-ERGIC-53 IgG representing the endoplasmic reticulum (ER)-Golgi intermediate compartment (ERGIC) or mouse anti-LAMP-1 IgG to stain the *trans*-Golgi network (TGN)/lysosomes were applied. Secondary detection was done with the help of Cy3-labeled goat anti-mouse IgG (displayed in red). Protein 3 (p3) had a granular cytoplasmic distribution (FLAG/DAPI [4′,6′-diamidino-2-phenylindole] column) and partially colocalized with the cellular ERGIC (FLAG/ERGIC-53/DAPI) and the TGN marker (FLAG/TGN/DAPI). p4a and p4b were ubiquitously distributed throughout the cytoplasm and nucleus. p5 had a granular, cytoplasmic staining pattern and partially colocalized with the ERGIC-53 proteins. Areas of colocalization are yellow. (B) Western blot analysis using a mouse-anti-FLAG monoclonal antibody displayed protein bands at the expected sizes for p4a (12 kDa), p4b (29 kDa), and p5 (25 kDa). p3 revealed a band 5 kDa higher (16 instead of 11 kDa) than expected possibly due to posttranslational modifications. β-Actin (b-Actin) staining was applied as a loading control.

noglobulin G (IgG) as described previously (19). To specify the subcellular localization of proteins, a colocalization study with organelle marker antibodies was done as described before (19). Counterstaining of the marker proteins for the endoplasmic reticulum (ER)-Golgi intermediate compartment (ERGIC) representing the CoV budding site was performed with anti-ERGIC-53 IgG. The *trans*-Golgi network (TGN) and lysosomes were stained with anti-lysosome-associated membrane glycoprotein 1 (anti-LAMP-1) IgG. Immunofluorescence signals were analyzed by confocal laser scanning microscopy (Leica, SP5 SMD). The majority of cells expressing p3 and p5 had distinct granular cytoplasmic staining patterns (Fig. 1A, FLAG/DAPI [4′,6′-diamidino-2-phenylindole] column). Both proteins partially colocalized with the ERGIC marker (Fig. 1A, FLAG/ERGIC-53/DAPI column). Minor colocalizations were observed for p3 with the TGN protein LAMP-1 suggesting putative processing along the secretory pathway (Fig. 1A, FLAG/ERGIC-53/DAPI column). p5 mainly colocalized with the ERGIC marker, but not with LAMP-1, indicating a possible retention (Fig. 1A, FLAG/ERGIC-53/DAPI column). p4a and p4b showed a more diffuse cytoplasmic and partially nuclear distribution without any colocalization with the organelle marker proteins. Most observations corresponded to the *in silico* predictions as summarized in Table 1. In Western blot analysis (Fig. 1B), p4a (12 kDa) and p4b (29 kDa) showed bands at the expected positions, whereas p3 migrated slightly slower than predicted (16 instead of 11 kDa), possibly due to posttranslational modifications. The distinct band of p5 at 23 kDa was slightly lower than predicted (25 kDa).

After confirmation of protein expression, we investigated putative IFN antagonistic functions. Upon virus infection, the IFN induction pathway is triggered by dsRNA molecules (intermediates of viral replication) that can be sensed by cellular retinoic acid-inducible gene I product (RIG-I)-like helicases (RIG-I and melanoma differentiation-associated protein 5 [MDA5]) (20). Downstream signaling involves activation of IFN regulatory factor 3 (IRF-3). IRF-3 is phosphorylated and dimerizes before it enters the nucleus to upregulate alpha interferon (IFN-α) and beta interferon (IFN-β) gene transcription (21). Previously we found evidence that MERS-CoV inhibited IRF-3 activation and IFN-β transcription in human cell cultures (10, 11). We therefore analyzed whether the accessory proteins are involved in counteracting the type I IFN response. The rabies virus phosphoprotein (RVP) served as a control because of its known function as an inhibitor of IFN induction through prevention of IRF-3 phosphorylation (22). An IFN-β promoter activation luciferase assay was conducted first. HEK-293T cells were transfected with p125-FF (firefly [FF] luciferase under the control of the human IFN-β promoter), pRL-SV40 (simian virus 40 [SV40] promoter regulating *Renilla* luciferase [RL] expression) and the respective plasmids encoding accessory proteins (p3, p4a, p4b, or p5) as well as the RVP. Transfected purified total RNA from vesicular stomatitis virus (VSV)-infected cells was used as a dsRNA analogue, as it induces RIG-I- and MDA5-dependent activation of the IFN response (our unpublished observation). Figure 2A illustrates that p3 and p4b had no effects on the IFN promoter activation, whereas p5 induced a general reduction of SV40 promoter activity with an increased firefly-to-*Renilla* luciferase ratio compared to the empty vector (EV) control. This effect was independent of the IFN inducer and had already occurred upon transfection of p5, indicating a major influence of this protein on the general transcription level which was not further analyzed (data not shown). Only p4a was able to inhibit the activation of the IFN-β promoter to levels similar to those of the control RVP.

To assess the involvement of the canonical IRF-3 pathway in this process, a green fluorescent protein (GFP)–IRF-3 fusion protein was used to assess IRF-3 nuclear translocation as described elsewhere (23). IFN induction was done by infection with Rift Valley fever virus clone 13 (RVFV Cl 13) at a multiplicity of infec-

FIG 2 p4a inhibits the type I IFN induction and secretion. Empty vector (EV) pCAGGS and rabies virus phosphoprotein (RVP) were included in all experiments as negative and positive controls, respectively. (A) The IFN-β (IFN-b) promoter activation was measured in HEK-293T cells upon transfection of 0.75 μg p125-FF (firefly [FF] luciferase under the control of the human IFN-β promoter), 0.005 μg pRL-SV40 (simian virus 40 [SV40] promoter regulating *Renilla* luciferase [RL] expression), and the respective plasmids encoding accessory proteins (p3, p4a, p4b, and p5; 0.05 μg each) as well as the RVP. After 24 h, cells were again transfected with 1.25 μg VSV-RNA (total RNA from vesicular stomatitis virus-infected cells used as a dsRNA analogue) for stimulation of the IFN pathway. The luciferase readout was performed after 20 h. FF luciferase values reflecting IFN-β promoter activity were normalized to RL controls. Three independent experiments were performed in triplicate. The plus sign ($p5^{+}$) indicates that the FF/RL ratio is elevated due to the general reduction of the transcription level measured by RL. All depicted *P* values ($P < 0.0001$ [***], $P < 0.001$[**], and $P < 0.05$ [*]) were determined by one-way analysis of variance (ANOVA) followed by Dunnett's test (EV as the control). (B) For a GFP–IRF-3 translocation assay, MA-104 cells were cotransfected with 0.25 μg GFP–IRF-3 and either 0.75 μg RVP

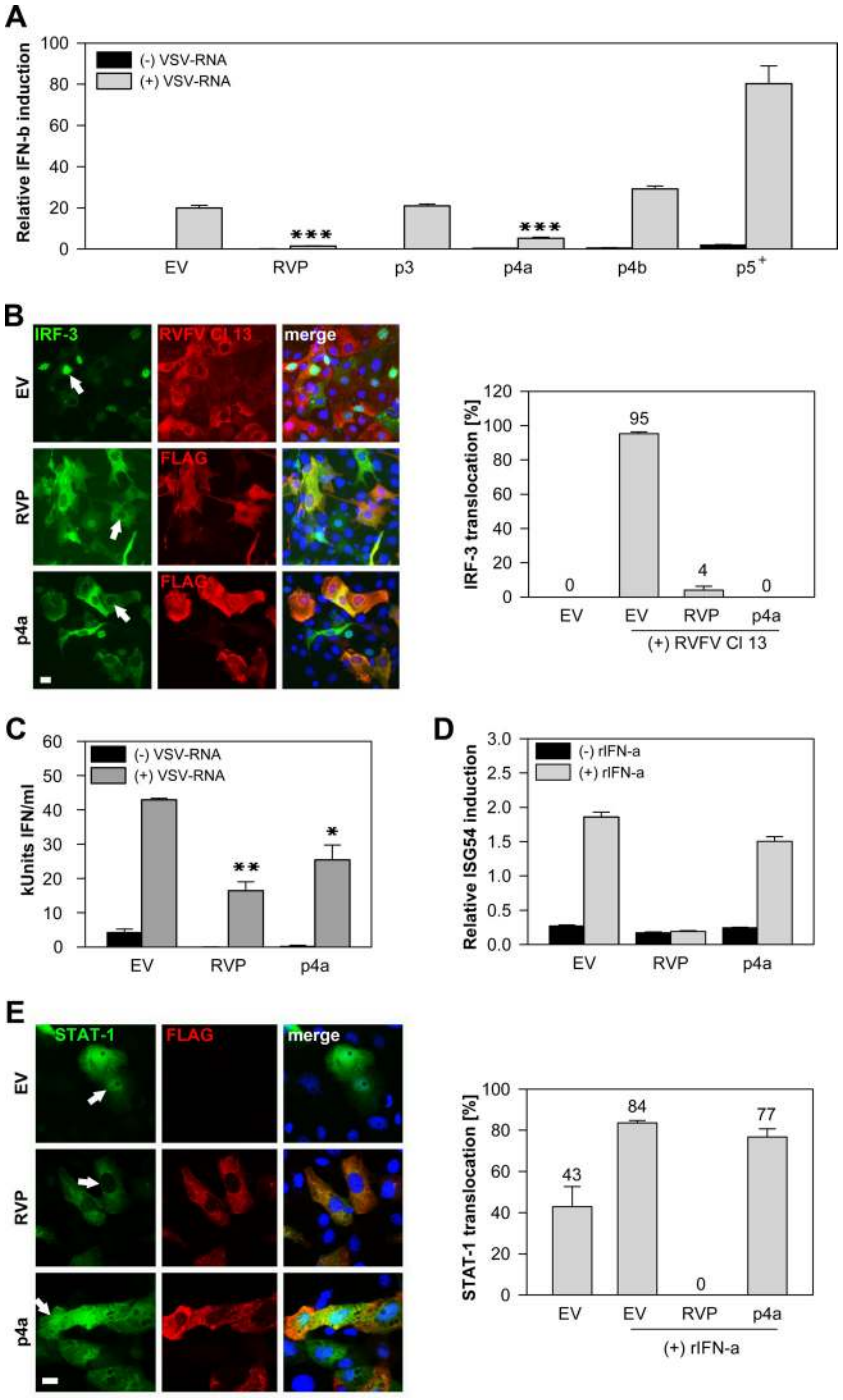

or p4a. After 24 h, the nuclear translocation of IRF-3 was induced by infection with RVFV Cl 13 (MOI of 5). Cells were fixed and stained with anti-FLAG IgG 8 h postinfection, and the number of translocation events was counted. Control cells transfected with an empty vector were stained with a polyclonal anti-RVFV IgG (38) to prove high infection efficiency. Depending on the number of transfected cells, at least three images were taken, and the total number of cells positive for GFP and FLAG was divided by the number of cells showing IRF-3 nuclear translocation. White arrows show representative cells expressing GFP–IRF-3 and RVP or p4a. Areas of coexpression are yellow. Analysis was done with a Motic Axiovision microscope (Zeiss). Bar, 10 μm. (C) MA-104 cells were transfected as indicated on the *x* axis. After 24 h, the cells were transfected with VSV-RNA (dsRNA analogue) to induce IFN production. Supernatants were collected after 20 h, and bioactive IFN was measured by adding supernatants onto cells for 7 h and infecting them with an IFN-sensitive RVFV Cl 13-RL reporter virus (26). Standard curves were done in parallel using recombinant pan-species IFN-α (rIFN-α). Error bars indicate standard deviations of three replicate samples of one of two independent experiments. kUnits, kilounits. (D) Vero cells were transfected with 0.75 μg pISG54-FF (FF under the control of the ISRE representing the ISG54 promoter), 0.005 μg pRL-SV40, and 0.05 μg RVP or p4a plasmid, and incubated with 2,000 U/ml rIFN-α. The luciferase readout was determined 20 h later. FF luciferase values of the ISG54 promoter activity were normalized to SV40 promoter-expressed RL (one of three independent experiments in triplicate). (E) For a STAT-1 nuclear translocation assay, Vero cells were transfected with 0.25 μg GFP–STAT-1, 0.25 μg pCAGGS, 0.25 μg RVP or p4a plasmid. Stimulation of the JAK/STAT signaling was done 24 h posttransfection by applying 1,000 U/ml rIFN-α. After 1 h, the cells were fixed and stained, and data were analyzed as demonstrated for panel B. Arrows indicate a representative cell coexpressing GFP–STAT-1 with RVP or p4a. Bar, 10 μm.

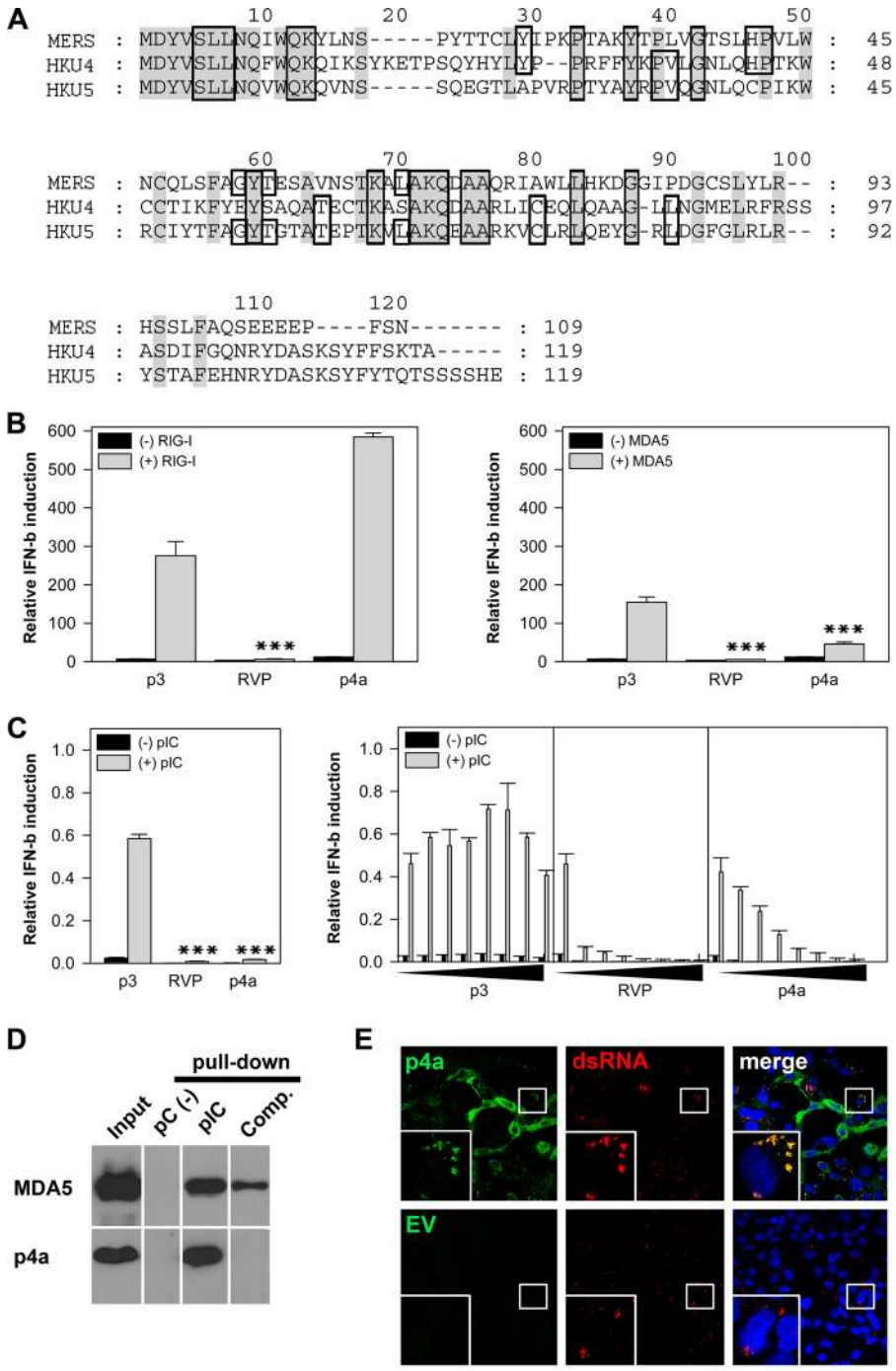

FIG 3 p4a inhibition of MDA5-dependent IFN induction and interaction with dsRNA. (A) Alignment of p4a amino acid sequence with the related betacoronaviruses (group C) bat CoV HKU4 and HKU5 (accession no. NC_009019.1 and NC_009020.1) including the predicted dsRNA-binding domains. Conserved amino acids are shown on a gray background, whereas the dsRNA-binding domain is boxed. Gaps introduced to maximize alignment are indicated by dashes. (B) An IFN-β promoter activation assay was performed 24 h after transfection with accessory protein 3 (p3) as a negative control, RVP (positive control) or p4a plasmid (0.05 μg) together with 0.1 μg RIG-I (left panel) or 0.1 μg MDA5 plasmid (right panel). The IFN-β reporter assay was done in three replicate samples using HEK-293T cells as described in the legend to Fig. 2A. Three experiments were done in triplicate. All depicted *P* values were determined by one-way analysis of variance (ANOVA) followed by Dunnett's test. (C) (Left) HEK-293T cells were transfected with 0.034 μg IFNbeta-Gluc (*Gaussia* luciferase [Gluc] under the control of IFN-β promoter) and 0.01 μg pEF1-Fluc (SV40 promoter regulating the firefly luciferase [Fluc] expression) and 0.025 μg plasmids encoding accessory protein 3 (p3), RVP, or p4a. To maintain an optimal stimulation of the IFN pathway, 0.006 μg of MDA5 plasmid was cotransfected. The total amount of DNA was constant (0.1 μg) by the addition of empty vector (pCAGGS). Transfection was performed with TransIT-LT1 (MirusBio) according to the instructions. After 12 h, the cells were again transfected with 0.1 μg poly(I·C) (pIC; Invivogen) for IFN-β promoter activation. The luciferase readout was performed 12 h after IFN induction. Gluc values reflecting IFN-β promoter activity were normalized to FF luciferase controls. Specifications refer to the 96-well format. (Right) To analyze dose-dependent IFN inhibition by p4a, the IFN promoter activation was measured as described above, but the amounts of p3, RVP, and p4a plasmids were increased from 0 to 0.05 μg. All experiments were performed three times in triplicate. (D) Poly(I·C)-coated agarose beads were prepared from poly(C)-coated

tion (MOI) of 5 guaranteeing infection of all transfected cells. RVFV Cl 13 has a truncated IFN antagonist (NSs) and was shown to induce IFN via IRF-3 (24). Figure 2B demonstrates that in all p4a-transfected cells, translocation of GFP–IRF-3 was inhibited 8 h postinfection with RVFV Cl 13 to an undetectable level. To investigate whether p4a-dependent inhibition of IRF-3 activation resulted in a reduced production of secreted IFN, a bioassay was performed as described previously (25, 26). The accumulated amount of IFN in cell supernatant of p4a-expressing and costimulated cells was reduced by 41% at 20 h posttransfection (Fig. 2C). Next it was determined whether p4a could also inhibit IFN signaling via the JAK/STAT pathway that is activated upon binding of IFN to the IFN-α/β receptor. JAK/STAT signaling leads to nuclear translocation of the IFN-stimulated gene factor 3 (ISGF3) complex comprising transcription factors STAT-1, STAT-2, and IRF-9 (8). ISGF3 binds to the IFN-stimulated response element (ISRE) promoter which regulates the transcription of ISGs (8). First, we conducted an ISRE-promoter activation luciferase assay. RVP, which is known to block the activation of STAT-1 (27), served as a positive control. Vero cells were transfected with reporter plasmids (pISG54-FF, including the ISRE promoter, pRL-SV40) and RVP or p4a plasmids, and incubated with recombinant IFN-α (PBL Interferon Source). p4a had minor effects in this assay compared to RVP, which inhibited the IFN signaling most efficiently (Fig. 2D). For further confirmation, a GFP–STAT-1 fusion protein was used in a nuclear translocation assay (28). While RVP completely prevented translocation of GFP–STAT-1 into the nucleus, p4a had only small inhibitory effects (Fig. 2E, right panel). We concluded that p4a had no or only a small influence on the IFN signaling pathway.

In silico analysis predicted that p4a had a dsRNA-binding domain (Table 1). Comparison with the other known group C betacoronaviruses, bat CoVs HKU4 and HKU5, indicated that the predicted dsRNA-binding domain was conserved between aa positions 5 to 90 (Fig. 3A). Notably, Ebola virus VP35 has a similar domain which is responsible for dsRNA silencing and sequestration, thereby blocking the activation of RIG-I-like helicases (RIG-I and MDA5) (18, 29). MDA5 is thought to be the main sensor for CoV recognition (30, 31), but RIG-I might also be involved (32). As MERS-CoV p4a has a putative dsRNA-binding domain and blocked IFN induction efficiently, we next investigated whether p4a reduces IFN-β promoter activation at the level of RIG-I-like helicases. For targeted IFN induction, the IFN-β promoter assays were performed with the same amount of RIG-I or MDA5 plasmid (250 ng) previously shown to activate downstream signaling (33) (Fig. 3B). For a negative control, we used p3, which had no effect on activation of the IFN pathway (Fig. 2A). As expected, with RVP, which is known to confer a downstream block at the level of IRF-3 activation (22), reduced IFN induction by both proteins (RIG-I and MDA5) was observed. Conversely, p4a had an enhancing effect on IFN promoter activation upon cotransfection with RIG-I (Fig. 3B, left panel), whereas activation triggered by MDA5 overexpression was reduced efficiently (Fig. 3B, right panel). To further specify the inhibition of p4a on MDA5 activation, IFN induction was additionally stimulated by transfection with poly(I·C), a main activator of MDA5 (20). Figure 3C (left panel) clearly demonstrates that only RVP and p4a strongly reduced the IFN induction upon poly(I·C) stimulation in comparison to the p3 negative control. This effect was dose dependent using plasmid concentrations ranging from 0 to 50 ng (Fig. 3C, right panel).

In the next step, we investigated whether p4a is able to bind to dsRNA molecules. MDA5, which is known to interact directly with poly(I·C), was applied as a positive control. In a pulldown experiment with poly(I·C) beads [negative-control poly(C) beads], it could be verified that p4a binds specifically to poly(I·C) (Fig. 3D). Binding could be completely blocked by poly(I·C) pretreatment of the lysates (Fig. 3D, right lane). To finally verify interaction of p4a with viral dsRNA, a protein-RNA colocalization assay was done with p4a-overexpressing and MERS-CoV-infected cells. As depicted in Fig. 3E, the expression pattern of p4a changed from a broad cytoplasmic distribution to a distinct pattern upon MERS-CoV infection, including fluorescence signals suggesting colocalization of p4a and viral dsRNA.

In summary, p4a acted as an efficient type I IFN antagonist blocking the IFN induction pathway. Its inhibitory effect on MDA5-dependent IFN activation, the direct interaction with poly(I·C), and the colocalization with viral dsRNA molecules strongly favor a block of MDA5 activation by dsRNA binding or sequestration. Several viral antagonists block MDA5 activation but have evolved a variety of mechanisms. Some have dsRNA-binding moieties leading to dsRNA sequestration as described for Ebola virus VP35 (29). Others, like the V protein of paramyxoviruses, interact with MDA5 and manipulate its folding to inhibit its activation (17). Interestingly, herpes simplex virus 1 antagonist US11 was observed to interact with MDA5 via its dsRNA-binding domain. The interaction between US11 and MDA5 was found to be RNA dependent (34). Further studies should therefore address whether p4a binds only dsRNA for sequestration or whether it also binds MDA5 and whether the binding to dsRNA influences the interaction with MDA5. Importantly, the p4a antagonism should be further assessed in the context of a full replicating virus to appreciate intravirus and virus-host protein interactions.

So far, no CoV IFN antagonists were shown to sequester dsRNA or bind MDA5 directly. However, mouse hepatitis virus (MHV) and SARS-CoV nucleocapsid proteins were able to block activation of dsRNA-triggered pathways by unknown mechanisms (35, 36). Most other CoV IFN antagonists were identified to counteract further downstream in the IFN induction pathway (37), emphasizing that MERS-CoV has presumably evolved a distinct mechanism to counteract the innate immune response.

beads (pC; Sigma) by incubating with 2 volumes of 2 mg of poly(I) (Sigma) per ml. Twenty microliters of a 25% agarose bead slurry was incubated with 400 μl cell extract of HEK-293T cells transfected with 2 μg plasmids expressing FLAG-tagged MDA5 or p4a. The cell extracts were supplemented with protease inhibitors (Roche). After incubation for 4 h at 4°C, the beads were pelleted by centrifugation, washed three times with lysis buffer, resuspended in SDS-PAGE loading buffer, boiled at 95°C for 5 min, and analyzed by Western blotting using anti-FLAG M2 antibody conjugated to horseradish peroxidase (HRP) (Sigma). PC-coated beads were included as specificity controls. For competition experiments (Comp.), pulldown reactions were supplemented with 10 μg of pIC (Invivogen). (E) For a protein-RNA colocalization study of p4a with viral dsRNA, Vero cells were transfected with 0.75 μg p4a or empty vector (EV) and infected with MERS-CoV (MOI of 1) 20 h later. After another 24 h, the cells were fixed and stained with rabbit anti-FLAG and mouse anti-dsRNA J2 IgG (39). Secondary detection was done with goat anti-rabbit Cy2 (green) and goat anti-mouse Cy3-labeled IgG (red). Yellow areas display colocalization of p4a signals with viral dsRNA.

ACKNOWLEDGMENTS

We are indebted to Ron Fouchier (Department of Viroscience, Erasmus Medical Center [MC], Rotterdam, The Netherlands) and Ali Zaki (Soliman Fakeeh Hospital, Kingdom of Saudi Arabia) for providing the MERS-CoV virus isolate. We are grateful to Artem Siemens for technical assistance, and we thank Daniel Ritz for critically reading the manuscript. We are thankful to Stephan Becker (University of Marburg), Takashi Fujita (Kyoto University), Adolfo García-Sastre (Mount Sinai Hospital, New York, NY), Luis Martinez (URMC Rochester), David E. Levy (NYUMC, New York, NY), and Klaus Conzelmann (LMU Munich) for providing p125-FF, pISG54-FF, pRL-SV40, GFP–STAT-1, GFP–IRF-3, RVP, and pCAGGS plasmids.

This study was supported by the European Union FP7 project EMPERIE (contract 223498), ANTIGONE (contract 278976), the German Research Foundation (DFG grant DR 772/3-1, MU3564/1-1), as well as the German Ministry of Education and Research (BMBF SARS II, 01KI1005A). F.W. was additionally funded under contracts 01KI0705 and We 2616/7-1. W.B. was supported by DFG grants BA3544/1-1 and SFB 704.

REFERENCES

1. **Rota PA, Oberste MS, Monroe SS, Nix WA, Campagnoli R, Icenogle JP, Penaranda S, Bankamp B, Maher K, Chen MH, Tong S, Tamin A, Lowe L, Frace M, DeRisi JL, Chen Q, Wang D, Erdman DD, Peret TC, Burns C, Ksiazek TG, Rollin PE, Sanchez A, Liffick S, Holloway B, Limor J, McCaustland K, Olsen-Rasmussen M, Fouchier R, Gunther S, Osterhaus AD, Drosten C, Pallansch MA, Anderson LJ, Bellini WJ.** 2003. Characterization of a novel coronavirus associated with severe acute respiratory syndrome. Science **300:**1394–1399.
2. **Zaki AM, van Boheemen S, Bestebroer TM, Osterhaus AD, Fouchier RA.** 2012. Isolation of a novel coronavirus from a man with pneumonia in Saudi Arabia. N. Engl. J. Med. **367:**1814–1820.
3. **World Health Organization.** 26 June 2013. Global Alert and Response. Middle East respiratory syndrome coronavirus (MERS-CoV)-update. World Health Organization, Geneva, Switzerland. http://www.who.int/csr/don/2013_06_26/en/index.html.
4. **Drosten C, Gunther S, Preiser W, van der Werf S, Brodt HR, Becker S, Rabenau H, Panning M, Kolesnikova L, Fouchier RA, Berger A, Burguiere AM, Cinatl J, Eickmann M, Escriou N, Grywna K, Kramme S, Manuguerra JC, Muller S, Rickerts V, Sturmer M, Vieth S, Klenk HD, Osterhaus AD, Schmitz H, Doerr HW.** 2003. Identification of a novel coronavirus in patients with severe acute respiratory syndrome. N. Engl. J. Med. **348:**1967–1976.
5. **Muller MA, Raj VS, Muth D, Meyer B, Kallies S, Smits SL, Wollny R, Bestebroer TM, Specht S, Suliman T, Zimmermann K, Binger T, Eckerle I, Tschapka M, Zaki AM, Osterhaus AD, Fouchier RA, Haagmans BL, Drosten C.** 2012. Human coronavirus EMC does not require the SARS-coronavirus receptor and maintains broad replicative capability in mammalian cell lines. mBio **3**(6):e00515–12. doi:10.1128/mBio.00515-12.
6. **Raj VS, Mou H, Smits SL, Dekkers DH, Muller MA, Dijkman R, Muth D, Demmers JA, Zaki A, Fouchier RA, Thiel V, Drosten C, Rottier PJ, Osterhaus AD, Bosch BJ, Haagmans BL.** 2013. Dipeptidyl peptidase 4 is a functional receptor for the emerging human coronavirus-EMC. Nature **495:**251–254.
7. **Perlman S, Dandekar AA.** 2005. Immunopathogenesis of coronavirus infections: implications for SARS. Nat. Rev. Immunol. **5:**917–927.
8. **Haller O, Kochs G, Weber F.** 2006. The interferon response circuit: induction and suppression by pathogenic viruses. Virology **344:**119–130.
9. **Kawai T, Akira S.** 2007. Antiviral signaling through pattern recognition receptors. J. Biochem. **141:**137–145.
10. **Kindler E, Jonsdottir HR, Muth D, Hamming OJ, Hartmann R, Rodriguez R, Geffers R, Fouchier RA, Drosten C, Muller MA, Dijkman R, Thiel V.** 2013. Efficient replication of the novel human betacoronavirus EMC on primary human epithelium highlights its zoonotic potential. mBio **4**(1):e00611–12. doi:10.1128/mBio.00611-12.
11. **Zielecki F, Weber M, Eickmann M, Spiegelberg L, Zaki AM, Matrosovich M, Becker S, Weber F.** 2013. Human cell tropism and innate immune system interactions of human respiratory coronavirus EMC compared to those of severe acute respiratory syndrome coronavirus. J. Virol. **87:**5300–5304.
12. **Narayanan K, Huang C, Makino S.** 2008. SARS coronavirus accessory proteins. Virus Res. **133:**113–121.
13. **Kopecky-Bromberg SA, Martinez-Sobrido L, Frieman M, Baric RA, Palese P.** 2007. Severe acute respiratory syndrome coronavirus open reading frame (ORF) 3b, ORF 6, and nucleocapsid proteins function as interferon antagonists. J. Virol. **81:**548–557.
14. **Frieman M, Yount B, Heise M, Kopecky-Bromberg SA, Palese P, Baric RS.** 2007. Severe acute respiratory syndrome coronavirus ORF6 antagonizes STAT1 function by sequestering nuclear import factors on the rough endoplasmic reticulum/Golgi membrane. J. Virol. **81:**9812–9824.
15. **van Boheemen S, de Graaf M, Lauber C, Bestebroer TM, Raj VS, Zaki AM, Osterhaus AD, Haagmans BL, Gorbalenya AE, Snijder EJ, Fouchier RA.** 2012. Genomic characterization of a newly discovered coronavirus associated with acute respiratory distress syndrome in humans. mBio **3**(6):e00473–12. doi:10.1128/mBio.00473-12.
16. **Voss D, Kern A, Traggiai E, Eickmann M, Stadler K, Lanzavecchia A, Becker S.** 2006. Characterization of severe acute respiratory syndrome coronavirus membrane protein. FEBS Lett. **580:**968–973.
17. **Motz C, Schuhmann KM, Kirchhofer A, Moldt M, Witte G, Conzelmann KK, Hopfner KP.** 2013. Paramyxovirus V proteins disrupt the fold of the RNA sensor MDA5 to inhibit antiviral signaling. Science **339:**690–693.
18. **Cardenas WB, Loo YM, Gale M, Jr, Hartman AL, Kimberlin CR, Martinez-Sobrido L, Saphire EO, Basler CF.** 2006. Ebola virus VP35 protein binds double-stranded RNA and inhibits alpha/beta interferon production induced by RIG-I signaling. J. Virol. **80:**5168–5178.
19. **Muller MA, van der Hoek L, Voss D, Bader O, Lehmann D, Schulz AR, Kallies S, Suliman T, Fielding BC, Drosten C, Niedrig M.** 2010. Human coronavirus NL63 open reading frame 3 encodes a virion-incorporated N-glycosylated membrane protein. Virol. J. **7:**6.
20. **Kato H, Takahasi K, Fujita T.** 2011. RIG-I-like receptors: cytoplasmic sensors for non-self RNA. Immunol. Rev. **243:**91–98.
21. **Fitzgerald KA, McWhirter SM, Faia KL, Rowe DC, Latz E, Golenbock DT, Coyle AJ, Liao SM, Maniatis T.** 2003. IKKepsilon and TBK1 are essential components of the IRF3 signaling pathway. Nat. Immunol. **4:**491–496.
22. **Brzozka K, Finke S, Conzelmann KK.** 2005. Identification of the rabies virus alpha/beta interferon antagonist: phosphoprotein P interferes with phosphorylation of interferon regulatory factor 3. J. Virol. **79:**7673–7681.
23. **Basler CF, Mikulasova A, Martinez-Sobrido L, Paragas J, Muhlberger E, Bray M, Klenk HD, Palese P, Garcia-Sastre A.** 2003. The Ebola virus VP35 protein inhibits activation of interferon regulatory factor 3. J. Virol. **77:**7945–7956.
24. **Billecocq A, Spiegel M, Vialat P, Kohl A, Weber F, Bouloy M, Haller O.** 2004. NSs protein of Rift Valley fever virus blocks interferon production by inhibiting host gene transcription. J. Virol. **78:**9798–9806.
25. **Biesold SE, Ritz D, Gloza-Rausch F, Wollny R, Drexler JF, Corman VM, Kalko EK, Oppong S, Drosten C, Muller MA.** 2011. Type I interferon reaction to viral infection in interferon-competent, immortalized cell lines from the African fruit bat Eidolon helvum. PLoS One **6:**e28131. doi:10.1371/journal.pone.0028131.
26. **Kuri T, Habjan M, Penski N, Weber F.** 2010. Species-independent bioassay for sensitive quantification of antiviral type I interferons. Virol. J. **7:**50.
27. **Brzozka K, Finke S, Conzelmann KK.** 2006. Inhibition of interferon signaling by rabies virus phosphoprotein P: activation-dependent binding of STAT1 and STAT2. J. Virol. **80:**2675–2683.
28. **Munoz-Jordan JL, Laurent-Rolle M, Ashour J, Martinez-Sobrido L, Ashok M, Lipkin WI, Garcia-Sastre A.** 2005. Inhibition of alpha/beta interferon signaling by the NS4B protein of flaviviruses. J. Virol. **79:**8004–8013.
29. **Kimberlin CR, Bornholdt ZA, Li S, Woods VL, Jr, MacRae IJ, Saphire EO.** 2010. Ebolavirus VP35 uses a bimodal strategy to bind dsRNA for innate immune suppression. Proc. Natl. Acad. Sci. U. S. A. **107:**314–319.
30. **Roth-Cross JK, Bender SJ, Weiss SR.** 2008. Murine coronavirus mouse hepatitis virus is recognized by MDA5 and induces type I interferon in brain macrophages/microglia. J. Virol. **82:**9829–9838.
31. **Zust R, Cervantes-Barragan L, Habjan M, Maier R, Neuman BW, Ziebuhr J, Szretter KJ, Baker SC, Barchet W, Diamond MS, Siddell SG, Ludewig B, Thiel V.** 2011. Ribose 2′-O-methylation provides a molecular

signature for the distinction of self and non-self mRNA dependent on the RNA sensor Mda5. Nat. Immunol. **12:**137–143.
32. **Li J, Liu Y, Zhang X.** 2010. Murine coronavirus induces type I interferon in oligodendrocytes through recognition by RIG-I and MDA5. J. Virol. **84:**6472–6482.
33. **Childs K, Randall R, Goodbourn S.** 2012. Paramyxovirus V proteins interact with the RNA helicase LGP2 to inhibit RIG-I-dependent interferon induction. J. Virol. **86:**3411–3421.
34. **Xing J, Wang S, Lin R, Mossman KL, Zheng C.** 2012. Herpes simplex virus 1 tegument protein US11 downmodulates the RLR signaling pathway via direct interaction with RIG-I and MDA-5. J. Virol. **86:**3528–3540.
35. **Ye Y, Hauns K, Langland JO, Jacobs BL, Hogue BG.** 2007. Mouse hepatitis coronavirus A59 nucleocapsid protein is a type I interferon antagonist. J. Virol. **81:**2554–2563.
36. **Lu X, Pan J, Tao J, Guo D.** 2011. SARS-CoV nucleocapsid protein antagonizes IFN-beta response by targeting initial step of IFN-beta induction pathway, and its C-terminal region is critical for the antagonism. Virus Genes **42:**37–45.
37. **Totura AL, Baric RS.** 2012. SARS coronavirus pathogenesis: host innate immune responses and viral antagonism of interferon. Curr. Opin. Virol. **2:**264–275.
38. **Habjan M, Pichlmair A, Elliott RM, Overby AK, Glatter T, Gstaiger M, Superti-Furga G, Unger H, Weber F.** 2009. NSs protein of Rift Valley fever virus induces the specific degradation of the double-stranded RNA-dependent protein kinase. J. Virol. **83:**4365–4375.
39. **Weber F, Wagner V, Rasmussen SB, Hartmann R, Paludan SR.** 2006. Double-stranded RNA is produced by positive-strand RNA viruses and DNA viruses but not in detectable amounts by negative-strand RNA viruses. J. Virol. **80:**5059–5064.
40. **Hofmann K, Stoffel W.** 1993. TMbase - a database of membrane spanning proteins segments. Biol. Chem. Hoppe-Seyler **374:**166.
41. **Emanuelsson O, Nielsen H, Brunak S, von Heijne G.** 2000. Predicting subcellular localization of proteins based on their N-terminal amino acid sequence. J. Mol. Biol. **300:**1005–1016.
42. **Horton P, Park KJ, Obayashi T, Fujita N, Harada H, Adams-Collier CJ, Nakai K.** 2007. WoLF PSORT: protein localization predictor. Nucleic Acids Res. **35:**W585–W587.